Desalination and Water Treatment
www.deswater.com

doi: 10.5004/dwt.2019.23249

138 (2019) 1–11
January

Enhancement of the thermal stability and mechanical properties of nanocrystalline cellulose/polyvinylidene fluoride ultrafiltration membranes by addition of graphene oxide

Qinfeng Zou, Xuejiao Liu, Tianhao Wang, Liping Zhang*

MOE Engineering Research Center of Forestry Biomass Materials and Bioenergy, College of Materials Science and Technology, Beijing Forestry University, No. 35 Tsinghua East Road, Haidian District, Beijing 100083, China;
emails: zhanglp418@163.com (L. Zhang), 358679919@qq.com (Q. Zou), 2436194688@qq.com (X. Liu), 2782414765@qq.com (T. Wang)

Received 1 March 2018; Accepted 4 October 2018

ABSTRACT

In this work, nanocrystalline cellulose (NCC)/polyvinylidene fluoride (PVDF) ultrafiltration composite membranes reinforced with graphene oxide (GO) were successfully prepared by the Loeb–Sourirajan phase inversion process. Firstly, the effects of mutual interactions between GO and NCC on membrane surface structure, morphology, and performance were investigated in detail. The existence of hydrogen bonds between GO and NCC in the membrane was confirmed by Fourier-transform infrared spectroscopy. The morphology of the membranes was observed by scanning electron microscopy. The water flux, bovine serum albumin rejection, and attenuate coefficient of the membranes were determined to investigate the filtration performance, and the filtration performance was hardly affected with addition of GO. The NCC/PVDF membrane modified with 1.0 wt% GO showed the highest tensile strength of 9.56 MPa, which was 58.01% higher than that of the unmodified membrane. Thermogravimetric analysis indicated that the blend membranes modified with GO had higher thermal stability compared with the unmodified NCC/PVDF membrane. When the NCC content was 0.5 wt% and the GO content was 1.0 wt% (the content of GO was based on the weight of PVDF), the optimized performance could be obtained due to the formation of hydrogen bonds between GO and NCC.

Keywords: Graphene oxide; Nanocrystalline cellulose; Polyvinylidene fluoride; Ultrafiltration membranes

1. Introduction

Ultrafiltration (UF) technology has attracted much attention in recent decades, which has been extensively used in various industrial fields, such as water desalination, ultrapure water production, product recycling, and wastewater treatment [1–5]. Hydrophilicity and porous structure of the membranes are essential for the fabrication of UF membrane [6]. The porous membrane used in these processes must have high permeability, nice hydrophilicity, and excellent chemical resistance to the feed streams [7]. Due to the easily controllable morphology and high porosity, polyvinylidene fluoride (PVDF) is extensively used for UF membranes preparation [8–11], which is a polymer with high thermal stability, high mechanical strength, and excellent chemical resistance to aggressive reagents, such as organic solvents, acids, and bases. However, there is a great drawback for PVDF membranes, that is, their hydrophobic nature, which can cause severe membrane fouling and low permeability, restricting their application in water and wastewater treatment [12–15]. Therefore, it is necessary for PVDF membranes to tune their surface hydrophilicity and improve their antifouling property [16]. Consequently, considerable efforts have been made to improve the hydrophilicity and fouling-resistant properties of PVDF membranes, including blending modification

* Corresponding author.

and surface modification. The ongoing development of surface modification has enabled integration of hydrophilic or superhydrophilic materials into the membrane surface by grafting or coating strategies [17], thereby the comprehensive performance of polymeric membranes is improved [18]. However, most surface coating and surface grafting techniques result in flux reduction and unsustainability of the functional layer. Blending modification is a practical method for surface modification, and it does not require any pre- or posttreatment procedures [19]. Recently, nanoparticle blending modification of polymer matrices has been investigated, and the modified polymer matrices exhibit superior performance to pure polymeric membranes [20,21]. However, the compatibility of the nanoparticles is extremely important for the membrane performance in PVDF solution.

Cellulose, as an abundant, cheap, biodegradable, and renewable resource, has gained much attention with the increasing interest in plant fiber blend materials [22]. Especially, nanocrystalline cellulose (NCC) has the features of hydrophilicity and nanoparticles including very large specific surface area, high mechanical strength, and high tensile modulus [23], which can be applied to UF. According to previous reports, NCC has been incorporated with polysulfone, polyether sulfone, or PVDF to enhance the hydrophilicity and mechanical properties of the membranes [3,24,25]. However, due to the high hydrophilicity and low miscibility in solvents of low or no polarity, there is a strong aggregation tendency for NCC in hydrophobic polymer matrix, impeding its feasible application in the UF technology [26]. Hence, some approaches have been devoted to address such problems, including amphiphilic diblock copolymer doping [27], and combining with carbon materials [28,29]. In particular, the combination of NCC with graphene oxide (GO) is considered as a practical way to conquer the abovementioned problems due to their unique properties [30].

Covalent functionalization on the surface of graphene is one strategy to fabricate graphene-based polymer blends, and it is an effective method to improve the interfacial interaction between graphene and the polymer matrix [31,32]. GO is a modified version of graphene with oxygen and hydrogen atoms bonded to the carbon atoms. Usually, GO is obtained by oxidizing graphene with strong acids and oxidizers [33]. The oxidation process introduces several functional groups into the graphene lattice, such as hydroxyl, epoxy, and carboxyl groups. The presence of oxygen and hydrogen-based functional groups enables the nanosheets of GO to disperse well in water and other organic solvents, which facilitates preparation of GO-containing membranes [34,35]. In some previous works, the influence of GO on thermal stability, permeation, and antifouling performances of UF membranes has been investigated [20,36]. Other scholars found that GO is also an ideal nanomaterial for attaching NCC and enhancing the mechanical properties and thermal stability of GO/NCC. The coupling of GO and NCC preparation of GO/NCC nanocomposites has been verified well in previous studies [28,29,37,38]. Thus, the GO/NCC nanocomposites have excellent mechanical properties and thermal stability, which can potentially be used as a reinforcing material for polymers.

Based on this conception and the body of previous research, the objective of this work is to prepare UF composite membranes with the addition of different GO ratios via phase inversion method and study the synergistic effects of NCC and GO nanomaterials in the matrix on the thermal and mechanical properties of the GO/NCC/PVDF UF composite membranes. These results offer a novel yet simple and effective way of designing UF composite membranes with extraordinary performance by incorporating with two nanomaterials. Membrane characterizations were confirmed in terms of scanning electron microscopy (SEM), thermogravimetric analysis (TGA), pulling force instrument, pure water flux, rejection, and others. Our results demonstrate that the GO/NCC/PVDF UF composite membranes showed some potential to be used as filtration membrane for water purification and/or wastewater treatment due to their structural stability and enhanced thermal/mechanical properties.

2. Experimental procedure

2.1. Materials and methods

The PVDF (T.P.) was purchased from the Dongguan City Special Exhibition of Plastic Raw Material Co., Ltd. (Dongguan, China). Polyvinylpyrrolidone K-30 (CP) and bovine serum albumin (BSA, BR: 98%) were purchased from Shantou Exiling Chemical Plant (Shantou, China) and Beijing Aoboxing Biological Technology Co., Ltd. (Beijing, China), respectively. Bamboo cellulose pulp (DP: 850–1,000) and GO (BR: ≥98%) were provided by Shandong Huatai Paper Mill (Shandong, China) and Jining Leader Nano Technology, Co., Ltd. (Jining, China), respectively. Sulfuric acid (H_2SO_4, 95%–98%), and N,N-dimethylacetamide (DMAc, CP) were purchased from Sinopharm Chemical Reagent Beijing Co., Ltd. (Beijing, China).

2.2. Preparation of NCC

Bamboo cellulose pulp was immersed in H_2SO_4 (25 wt%) solution under mechanical stirring at 85°C for 4 h, and the solid to liquid ratio was 1:40. After the end of the reaction, the pH of the solution was regulated until it was neutral by adding deionized water. After sieving and drying, the solids were immersed into DMAc and homogenized with a high-pressure homogenizer (NS1001S2K, GEA Niro Soavi Co., Italy) at a high pressure of 100 MPa. Through this process, the NCC was dispersed well into DMAc.

2.3. Preparation of the blend membranes

The possible membrane formation mechanism affected by the synergetic effect between the GO and NCC are presented in Fig. 1. The membranes were prepared by the Loeb–Sourirajan phase inversion process. The GO (0, 0.5, 1.0, 1.5, and 2.0 wt% based on the weight of PVDF) nanomaterials was first added to NCC/DMAc solution. The solution was sonicated for 10 h, and PVDF was then dissolved in the GO/NCC/DMAc solution. This casting solution was obtained by swaying at 70°C under mixing with an electric blender for 24 h. After stirring, the solutions were sealed and stored at room temperature for up to 24 h to remove the bubbles. A small amount of each casting solution (Table 1) was then poured onto a clean glass plate and scraped with a homemade scraper. After exposed to air atmosphere for 10 s, the resultant membranes were soaked in distilled water for

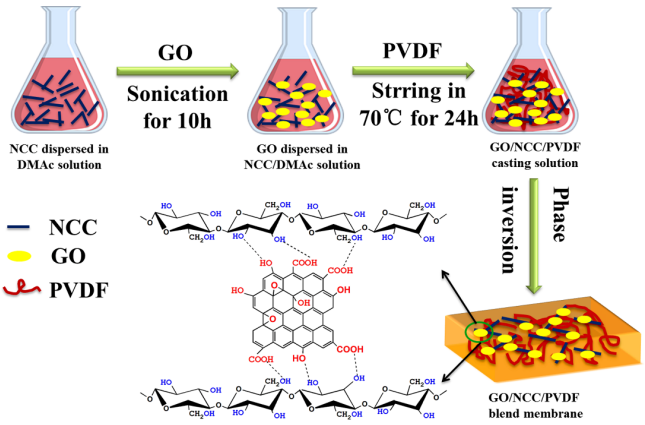

Fig. 1. The possible membrane formation mechanism affected by the synergetic effect between GO and NCC.

Table 1
Compositions of the casting solutions (the content of GO was based on the weight of PVDF)

Membrane type	PVDF (wt%)	PVP (wt%)	NCC (wt%)	GO (wt%)	DMAc (wt%)
M0	14	0.3	0.5	–	85.2
M1	14	0.3	0.5	0.5	85.2
M2	14	0.3	0.5	1.0	85.2
M3	14	0.3	0.5	1.5	85.2
M4	14	0.3	0.5	2.0	85.2

24 h to accomplish phase transformation and air-dried before characterization.

2.4. Materials characterization

Transmission electron microscopy (TEM, JEM-1010, JEOL, Japan) was used to determine the morphology of the NCC, GO, and GO/NCC with an accelerating voltage of 80 KV. To enhance contrast in TEM, the NCC was negatively stained with a 2 wt% aqueous solution of phosphotungstic acid for 1 min. Nitrogen adsorption–desorption isotherms were determined by using Brunauer–Emmett–Teller (BET) method using Micromeritics ASAP-2460 (Shanghai), and GO was degassed at 50°C for several hours. And, the specific surface area of the GO was determined by employing the BET equation. The dimension of GO was examined using atomic force microscope (AFM), and the GO was dispersed by sonication in water solution, then dried and tested under non-contact mode.

2.5. Fourier-transform infrared spectroscopy

The membrane samples were completely dried at 50°C in a drying oven, and then KBr pellets were prepared for analysis. Before testing by Fourier-transform infrared (FTIR) spectroscopy (Tensor 27, Bruker, Ettlingen, Germany), the KBr pellets were placed on the sample holder. All of the spectra were recorded in the wave number ranging 400–4,000 cm^{-1}.

2.6. Scanning electron microscopy

The GO/NCC/PVDF and NCC/PVDF blend membranes were broken down in nitrogen liquid. After spraying with gold, the fractured cross-sections and bottom surfaces of the membranes were observed by SEM (S-3000n, Hitachi, Japan).

2.7. Thermogravimetric analysis

The thermal stability of the membranes was investigated by TGA (TGA-600, Shimadzu, Japan). The experiments were performed under an N_2 atmosphere (20 mL/min). The temperature was increased from room temperature to 600°C at a heating rate of 10°C/min.

2.8. Mechanical properties

A tensile testing machine (DCP-KZ300, Sichuan, China) was used to test the tensile strength and elongation-at-break of the membranes. The speed of the cross head was 20 mm/min. The dried membranes were cut into rectangles with a width of 15 mm and a total length of 100 mm. All of the membrane samples were tested under ambient conditions. To minimize the experimental error, the reported values were the average of five samples.

2.9. Contact angle characterization and surface energy

The hydrophilicity of the dry membranes was examined using a water contact angle measuring instrument (GBX Instruments, Germany). A sessile drop was formed on the membrane surface by slowly and steadily depositing 5 μL of water with a microsyringe. The contact angle was measured at the membrane–water–air interphase at room temperature within 10 s of addition of the water drop. For each sample, measurements were performed at six locations and the values were averaged. From the contact angle measurements, the surface energy ω_A was calculated as follows:

$$\omega_A = \gamma_w\left(1+\cos\theta\right) \tag{1}$$

where γ_W was the surface tension (7.28×10^{-2} N/m).

2.10. Pure water flux and BSA rejection

The pure water flux of the membranes was determined based on the previous methods [39]. Initially, the membrane samples were compacted at an operating pressure of 0.15 MPa with pure water for 30 min. The volume of filtered water (m^3) in some portions of the membrane was obtained with working pressure of 0.1 MPa and working time t (h). All the filtration experiments were carried out under this pressure, and the permeated was collected every 5 min. To minimize the investigation error, seven samples were fabricated for each type of membrane and measured, and the average flux data were reported. The pure water flux J_W (L/(m^2·h)) was calculated as follows:

$$J_w = \frac{V}{\left(A\cdot t\right)} \tag{2}$$

where V was the volume of filtered water (m^3), A was the membrane area (m^2), and t was the working time (h).

The rejection of BSA solution (1 g/L) was tested under a working pressure of 0.1 MPa. The absorbance of the filtered solution was measured at 280 nm with a UV-1801 ultraviolet–visible spectrophotometer (Third Analysis Apparatus Co., Shanghai, China). The rejection R (%) was calculated as follows:

$$R = \left(1 - \frac{A_f}{A_i}\right) \times 100\% \tag{3}$$

where A_f and A_i were the absorbance of the filtered and initial solutions, respectively.

2.11. Antifouling performance

First, the initial pure water flux of the membrane J_i (L/(m^2·h)) was measured before the UF process. Second, BSA solution (1 g/L) was processed by the UF membrane for 1 h. The membrane was then cleaned with deionized water for 1 h. After the membrane cleaning step, the recovery pure water flux of the membrane J_r (L/(m^2·h)) was determined.

The pure water flux attenuation coefficient M (%) was calculated as follows:

$$M = \frac{(J_i - J_r)}{J_i} \times 100\% \tag{4}$$

3. Results and discussion

3.1. Transmission electron microscopy

The TEM was used to investigate the morphology of the NCC, GO, and GO/NCC composites; the NCC, GO, and GO/NCC nanocomposites were relatively uniformly dispersed in the DMAc. Fig. 2(a) shows TEM images of the NCC derived from bamboo cellulose pulp board; the size of the NCC was measured from the TEM images, which had lengths ranging from 500 to 700 nm, and widths ranging from 20 to 50 nm [40–42]. The NCC was prepared using the methods of dilute sulfuric acid hydrolysis and physical high-pressure homogenization in the range of aspect ratio from 10 to 35. According to their relatively high aspect ratios, the prepared NCC could be an effective reinforcement in nanocomposite for improving their mechanical properties [43]. The TEM micrograph images of GO is shown in Fig. 2(b). It is observed that GO had a wrinkled surface and wormlike structure, confirming the successful exfoliation of GO layers. The similar results were observed in the report of Safarpour et al. [44], and according to their results the films were folded or continuous at times and it was possible to distinguish the edges of individual sheets, including kinked and wrinkled areas. In order to measure the thickness of GO sheets, AFM observations were conducted. The tapping-mode AFM image of GO is presented in Fig. 2(e). From cross-section analysis, it was observed that GO had a height of 0.978 nm (Fig. 2(f)), corresponding well with the reported thickness found in previous

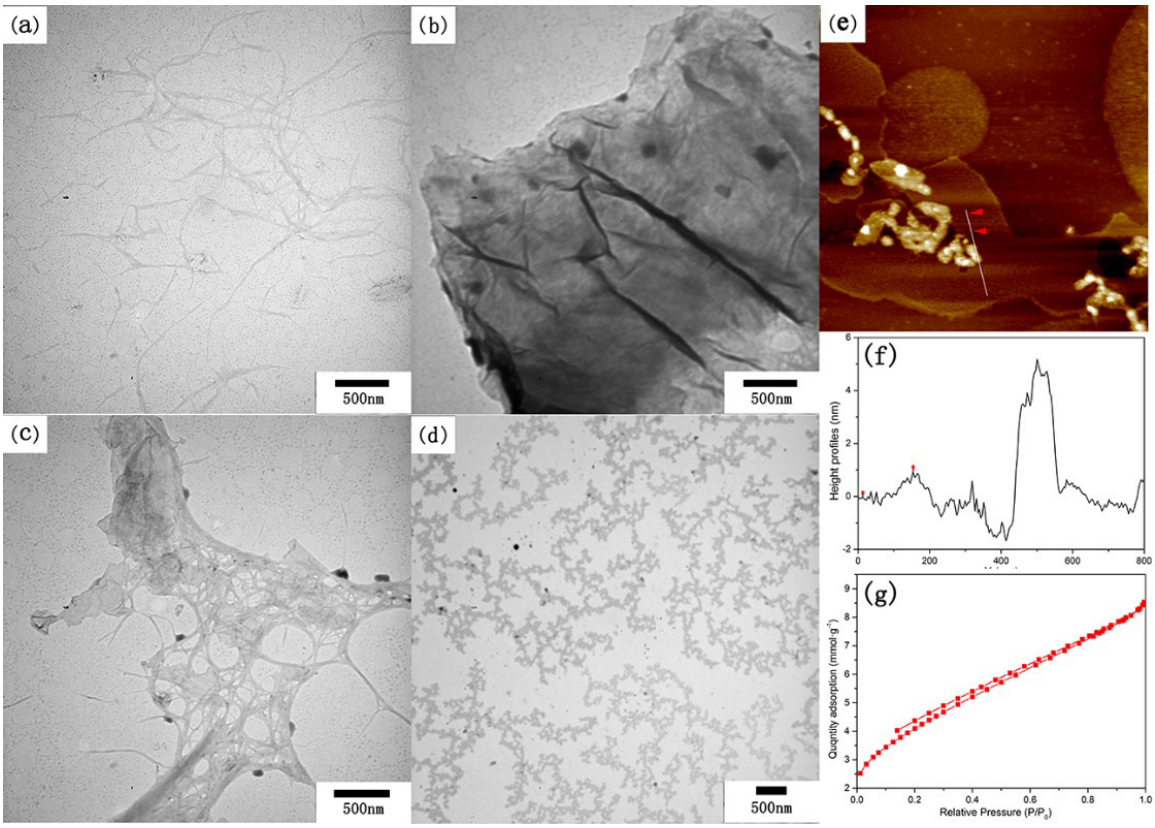

Fig. 2. TEM images of (a) NCC, (b) GO, (c) GO/NCC, (d) GO/NCC/PVDF, (e) AFM image of GO, (f) height profiles of GO sheets, and (g) N_2 adsorption–desorption isotherm of GO.

literature [45]. Moreover, the specific surface area of GO was determined by N_2 adsorption–desorption measurements. According to the nitrogen isotherm shown in Fig. 2(g), the surface area of GO was 334.05 m^2/g, which was calculated by BET equation. To further investigate the linkages between the GO and NCC molecule, the GO/NCC nanocomposite is shown in Fig. 2(c), revealing that GO was noticeably deposited on a weblike structure of NCC. This indicated that GO acts as anchoring sites for linking NCC due to the strong interaction between GO and NCC. It is considered that there was strong hydrogen bond link between the GO and NCC. In addition, this image implied that the compatibility between the GO and NCC was excellent enough to obtain nanosize dispersion. The TEM image of GO/NCC/PVDF in Fig. 2(d) shows that the GO/NCC/PVDF was uniformly distributed in DMAc solution. Based on Fig. 2(d) of TEM resulted above, it is concluded that the GO/NCC nanocomposites had good compatibility in PVDF matrix.

3.2. FTIR analysis

Fig. 3 shows the FTIR spectra of pure PVDF, pure GO, and the NCC/PVDF and GO/NCC/PVDF films. The FTIR spectrum of GO (Fig. 3(d)) exhibited two absorption bands at 1,737 and 1,618 cm^{-1}, which were assigned to the C=O stretching vibration of carboxyl group (COOH) and aromatic C=C skeletal vibration, respectively. The bands appeared at 1,263 and 1,051 cm^{-1} both represented the stretching vibrations of aliphatic C–O, and C–O stretching vibration in epoxy groups was also presented at 879 cm^{-1} [46], while the peak at 1,404 cm^{-1} could be assigned to the stretching and deformation vibration of aromatic C–OH [29]. Moreover, a broad –OH stretching band observed from 3,000 to 3,500 cm^{-1} appears in the spectra of both NCC/PVDF and GO/NCC/PVDF films, which was in accordance with results of Xu et al. [47]. In spectrum of the PVDF film (Fig. 3(a)), the peaks at 1,402 and 1,180 cm^{-1} could be attributed to the plane deformation (scissoring motion) of CH_2 groups and the C–C stretching vibration, respectively [48]. The peaks around 875 and 840 cm^{-1} are related to the C–C–C asymmetric stretching vibration and C–F stretching vibration, respectively. The spectrum of the NCC/PVDF blend film is similar to the film prepared from pure PVDF beside the –OH stretching peak at 3,355 cm^{-1}, indicating hydrophilic groups (–OH) provided by adding NCC. Compared with the spectrum of the NCC/PVDF film, the GO/NCC/PVDF film showed a broad C=O stretching vibration peak around 1,679 cm^{-1} in the spectra of GO/NCC/PVDF film (Fig. 3(c)), indicating the successful incorporation of GO. In addition, the peak at 3,355 cm^{-1} became broadened and the relative intensity of the C–O stretching vibration changes in the GO/NCC/PVDF film as well. Moreover, the peak corresponding to the –C=O skeletal vibration shifted to a lower wavenumber (from 1,737 to 1,679 cm^{-1}), indicating the hydrogen bond link between GO and NCC [28]. It was noteworthy that the functionality of nanocomposite depends not only on the natural properties of each component, but also on the synergistic effect between them. An effective interaction, such as hydrogen bonding, between GO and NCC was important for mechanical properties of the blend films. It also indicated that there is good miscibility between GO and NCC [28,49,50].

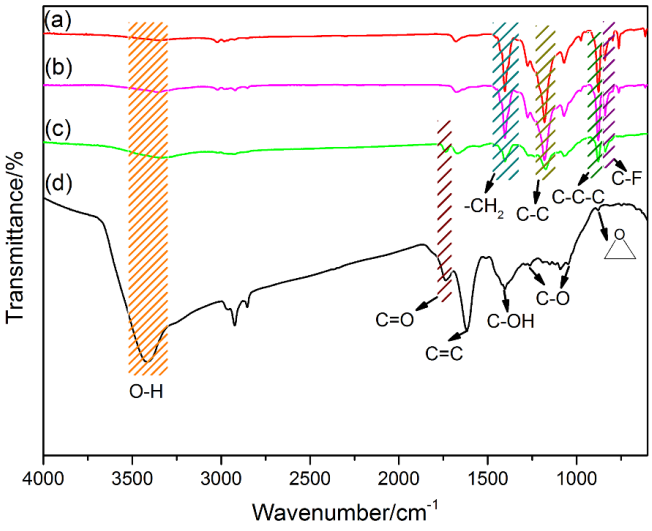

Fig. 3. FTIR spectra of (a) PVDF, (b) NCC/PVDF, (c) GO/NCC/PVDF, and (d) GO.

3.3. Morphologies of the membranes

To investigate the effect of the GO content on the membrane structure, SEM was performed to observe the surface and cross-sectional morphologies of the various membranes. The SEM images of the blend membranes with various GO contents are shown in Fig. 4. Regarding to the cross-sectional structure, all the membranes exhibited the typical asymmetric

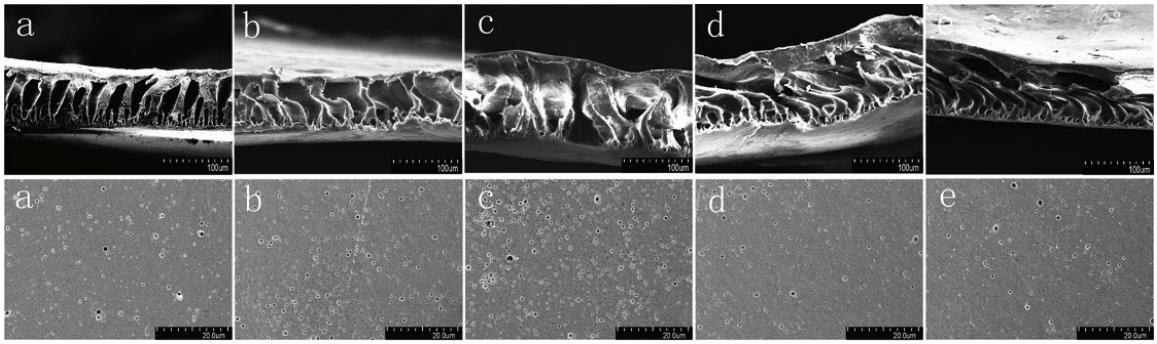

Fig. 4. SEM images of the cross-sections and upper surfaces of the blend membranes with (a) 0, (b) 0.5, (c) 1.0, (d) 1.5, and (e) 2.0 wt% GO.

structure, consisting of a skin layer as a selective barrier and a much thicker fingerlike substructure. The skin layer was relatively thin and compact, which resulted in the high resistance and low flux, and the fingerlike porous sublayer plays an important role for supplying mechanical strength [51]. This main reason for this phenomenon was the high mutual diffusivity of water and DMAc [52]. With the increasing GO in GO/NCC/PVDF membranes from 0.5 to 1.0 wt%, the pore size and porosity were slightly increased compared with NCC/PVDF membranes (Figs. 4(b) and (c)). As reported elsewhere, GO was one of the hydrophilic additives, which could expedite the solvent and non-solvent exchange rate during phase inversion process, resulting in the formation of larger pore channels [19,53,54]. This increased the roughness of the membrane and forms a dense hydrophilic layer, slightly enhancing the hydrophilicity of the blend membrane and the pure flux. However, the pore channel of GO/NCC/PVDF membranes became a spongelike structure compared with the other membranes, showing quite different structures in cross-sectional morphology when the content of GO increased from 1.0 to 2.0 wt% that contributed to the strong interaction between GO and NCC, which lead to agglomeration of the GO/NCC. Thus, the SEM images indicated that the moderate addition of GO influenced the NCC/PVDF membranes, thereby altering the pore density and pore diameter of surface micropores [12].

3.4. Thermogravimetric analysis

Thermal degradation of NCC/PVDF film and GO/NCC/PVDF films in nitrogen atmosphere is shown in Fig. 5. The effects of temperature variations on the behavior of material with the temperature heated up to 600°C from room temperature. The T_{onest} value was the initial decomposition temperature, and T_{max} was the temperature of the maximum decomposition rate. From Fig. 5(a), the thermal properties of GO/NCC/PVDF films with different amounts of GO indicated that all of the GO/NCC/PVDF films exhibited the same degradation pattern. And, the incorporation of GO had an apparent effect on the thermal degradation temperature of NCC/PVDF film. As seen in Fig. 5(b), the T_{onest} and T_{max} of all the GO/NCC/PVDF films were higher than that of the NCC/PVDF film. For example, the NCC/PVDF film, T_{onest} = 291°C, T_{max} = 456°C, there were two decomposition stages: 291°C–412°C, which was attributed to the decomposition of NCC, and 412°C–506°C, which was attributed to the decomposition of PVDF. For the GO/NCC/PVDF films with 0.5 wt% GO, T_{onest} =352°C, T_{max} =482°C, there also were two decomposition stages: 352°C–445°C, attributed to the decomposition of GO/NCC, and 445°C–530°C, attributed to the decomposition of PVDF. It was worth mentioning that T_{onest} and T_{max} of the GO/NCC/PVDF films with 0.5 wt% GO loading were about 61°C and 26°C higher than that of the NCC/PVDF film, respectively. These results indicated that the GO flakes could improve the thermal stability of NCC/PVDF because the mobility of the polymer segments at the interfaces of NCC/PVDF and GO flakes was suppressed by strong interactions between GO and NCC. Thus, inclusion of nanoscale fillers into the polymer matrix could enhance the thermal properties of the resultant blend [55,56]. However, the efficiency strongly depended on the dispersion, orientation, and intrinsic properties of the fillers and the interfacial interactions between the fillers

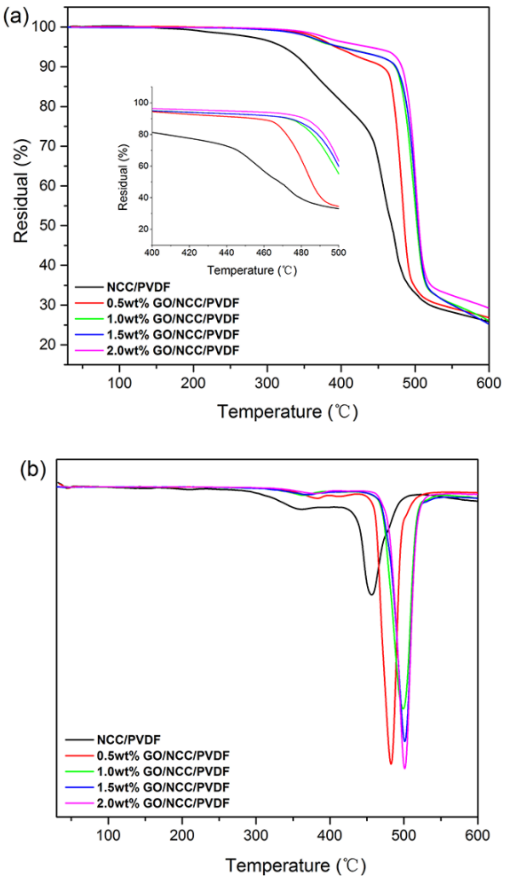

Fig. 5. (a) TGA and (b) DTG curves of the NCC/PVDF film and GO/NCC/PVDF films containing 0.5, 1.0, 1.5, and 2.0 wt% GO.

and the matrix [57]. From Fig. 5(a), the char yield of the GO/NCC/PVDF film was higher than that of the NCC/PVDF films because of the strong interaction between GO and NCC. For example, at 510°C, the char yield of the NCC/PVDF film was about 30%, whereas the char yield of the GO/NCC/PVDF film was 32%. This meant that some GO remains in the blend at high temperature. Thus, it was expected that the GO/NCC/PVDF blend film possesses better mechanical properties than the NCC/PVDF film at high temperature [29].

3.5. Mechanical properties

The results of tensile strength and elongation-at-break tests of the NCC/PVDF membrane and GO/NCC/PVDF membranes with different GO contents are shown in Fig. 6. Compared with the NCC/PVDF membranes, the tensile strengths of the GO/NCC/PVDF membranes were significantly improved. The tensile strength increased with increasing contents of GO up to 1.0 wt%, and then it gradually decreased. The noticeable trend was explained in terms of suitability of GO as a filler for the polymer materials, which was due to its excellent mechanical properties, high surface area, and high surface and high aspect ratio [48]. The GO in the casting solution began to aggregate when its concentration was higher (>1.0 wt%), causing the tensile strength to reduce. Furthermore, the elongation-at-break of the blend membranes had similar variation trends with the

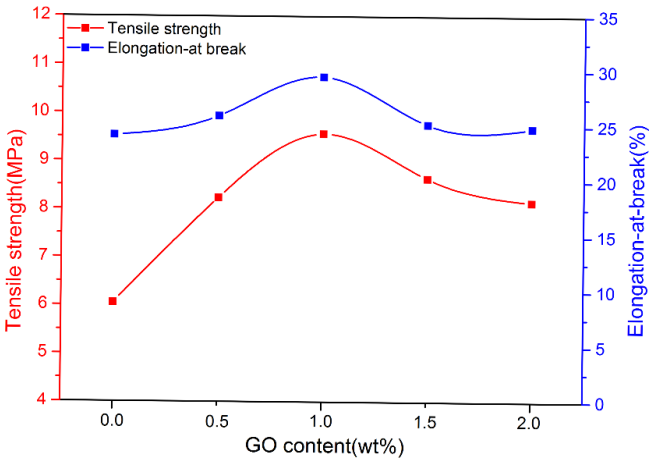

Fig. 6. Effect of GO loading on the tensile strength and elongation-at-break of the GO/NCC/PVDF.

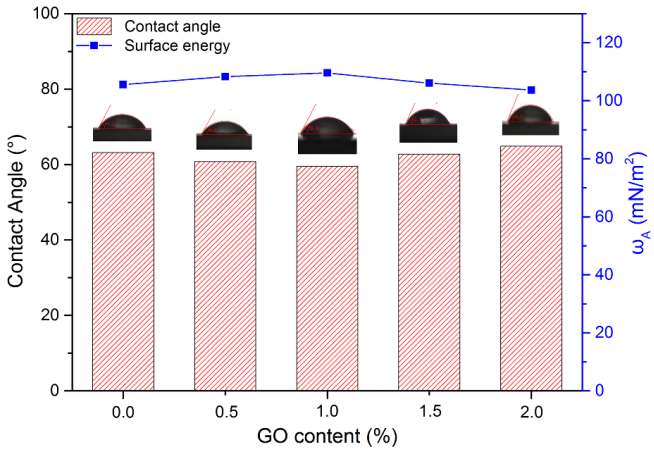

Fig. 7. Contact angles and surface energies of the blend membrane with GO contents of 0, 0.5, 1.0, 1.5, and 2.0 wt%.

tensile strength. These results demonstrated that adding GO into the NCC/PVDF membranes could cause the membrane strength and elasticity increased. Compared with 6.05 MPa and 24.18% for the NCC/PVDF membrane (increased by 58.01% and 21.96%, respectively), the highest tensile strength and elongation-at-break of the GO/NCC/PVDF membrane were 9.56 MPa and 29.49%. This was because both the static regularity of the planar construction and the hydrogen bonding interactions between GO and NCC act as an adhesive in the GO layers improved the crystallinity of the membranes, enhancing the mechanical strength and toughness [58]. Therefore, a hybrid membrane with good mechanical properties could be prepared by introducing an appropriate content of GO, which could be used under higher pressure conditions [59,60].

3.6. Contact angle characterization

The hydrophilicity of the membrane surfaces was investigated by water contact angle measurements (Fig. 7). The initial contact angle was measured immediately after the distilled water was dropped onto the membrane surface, which reflects the natural wettability of the blend membrane. Generally, the smaller the contact angle, the better the hydrophilicity and surface energy. From Fig. 7, The NCC/PVDF membranes possessed water contact angle of 63.2°, whereas GO/NCC/PVDF membranes with content of 0.5, 1.0, 1.5, and 2.0 wt% GO achieved water contact angle of 60.8°, 59.6°, 62.8°, and 64.9°, respectively. The amelioration of hybrid membrane hydrophilicity might be ascribed to the spontaneous migration of hydrophilic nanomaterials moving toward the membrane/water interface to decrease the interface energy during the phase inversion process [61–63]. When embedding 1.0 wt% of GO, the contact angle of GO/NCC/PVDF membranes decreased to the lowest, and a further increase of GO (more than 1.0 wt%) did not result in decrease in the contact angle. The reason could be explained as follows: on the one hand, the GO with high content greatly enhanced the electrostatic and π–π accumulation effect of GO, leading to the agglomeration of GO in casting solution [64]. On the other hand, the oxygen-containing functional groups on the surface of GO were reduced due to the hydrogen bond between GO and NCC [65]. All of these could cause agglomeration of GO. On the other hand, the interaction between GO and NCC certain reduced the hydrophilic groups of the GO/NCC nanocomposite. Note that all of the membranes with various GO loadings from 0 wt% to 2.0 wt% exhibited a similar contact angle of around 62°, which was not similar to previous research studies [19,48,59,66]. The reason is that when the loading of GO was no more than 1.0 wt%, the change of hydrophilic angle was not significant. It was mainly because that the hydrogen bond between oxygen fossil GO and NCC weakened the hydrophilic energy of GO/NCC/PVDF composite membrane [67]. However, when the loading of GO was over 1.0 wt% or even reached 2.0 wt%, the GO would have obvious agglomeration, which also weakened the hydrophilic energy of GO/NCC/PVDF composite membrane [68]. The influence of surface hydrophilicity was a significant factor in determining the flux and antifouling performance of membranes [53]. A compact water layer on the top surface of the blend membrane would hinder organic deposition on the blend membrane, which could improve the antifouling performance [51].

3.7. Pure water flux and rejection

The effects of the GO content of the GO/NCC/PVDF blend membrane on the permeability and BSA rejection are shown in Fig. 8, which suggest an obvious appearance that the GO/NCC/PVDF membranes revealed similar water permeation fluxes and separation efficiencies compared with NCC/PVDF membranes. According to Fig. 8, the highest pure water flux of GO/NCC/PVDF membranes was 204.75 L/(m²·h) with adding 1.0 wt% GO, being 9.3% higher than that of NCC/PVDF membranes (187.32 L/[m²·h]). This improvement was not obvious in the pure water flux due to the hydrogen bond interaction between GO and NCC effected the hydrophilic ability of composite membranes. As the contact angle shown in Fig. 7, the variation trend of contact angle was almost in accord with the trend of water permeability.

The BSA rejection properties of the NCC/PVDF and GO/NCC/PVDF blend membranes are also presented in Fig. 8. It was concluded that the rejection parameter of the

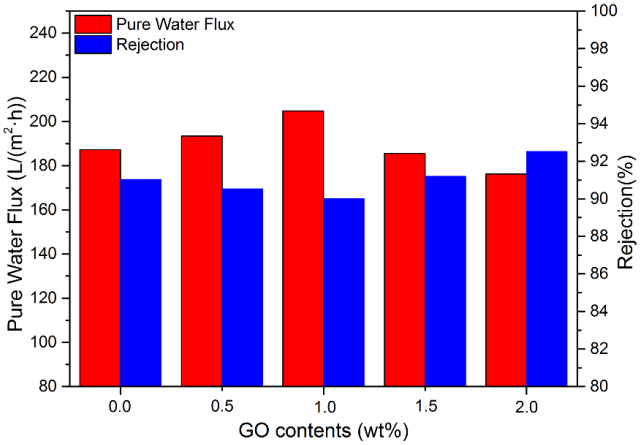

Fig. 8. Effect of the GO content on the pure water flux and BSA rejection ratio of the GO/NCC/PVDF membrane.

NCC/PVDF and GO/NCC/PVDF blend membranes was over 90%. These results might be explained by a combination of the small pore size of the skin layer of membranes (which was less than the size of BSA [69]) and the hydrophilicity based on the principle of the interfacial hydration layer as protective barrier membrane surface so as to hinder the protein molecules to penetrate through the hybrid membrane during the fouling or BSA filtration operating [66]. Moreover, the GO content had no significant effect on the BSA rejection of the blend membrane, which might be due to the surface hydrophilic groups were reduced by hydrogen bond interaction between GO and NCC [67], On the other hand, after adding GO, the changes in membrane surface pore not only improved the infiltration capacity of the blend membrane, but also reduced the interception capability trend of BSA molecules. This was because the GO provided an advantageous porous surface with a favorable inner structure of the membrane [70].

3.8. Antifouling performance

Cyclic filtration tests of the NCC/PVDF and GO/NCC/PVDF membranes were performed to determine the effect of GO on the fouling resistance. The initial pure water flux, BSA solution flux, and recovery of the pure water flux of the NCC/PVDF membrane and GO/NCC/PVDF membranes with the addition of different GO are shown in Fig. 9(a). Reversible protein adsorption leads to reversible fouling, which could be removed by simple hydraulic cleaning. In contrast, irreversible fouling was caused by strong adsorption of protein molecules on the surface or entrapment of protein molecules in the pores [71]. As shown in Figs. 9(a) and (b), the GO/NCC/PVDF membranes had similar antifouling performance to the NCC/PVDF membrane, but their antifouling performance was higher than that of the nascent PVDF membrane. One critical reason was that the ionized hydroxyl groups of NCC and hydroxyl/carboxyl groups of GO could interact with water molecules through Van der Waals force and hydrogen bonds for the formation of water molecular layer on GO/NCC/PVDF surface to avoid proteins deposition (adsorption) [72]. It was worth mentioning that the presence of hydrogen bonds between GO and NCC makes GO/NCC nanocomposites more evenly dispersed in PVDF matrix (as

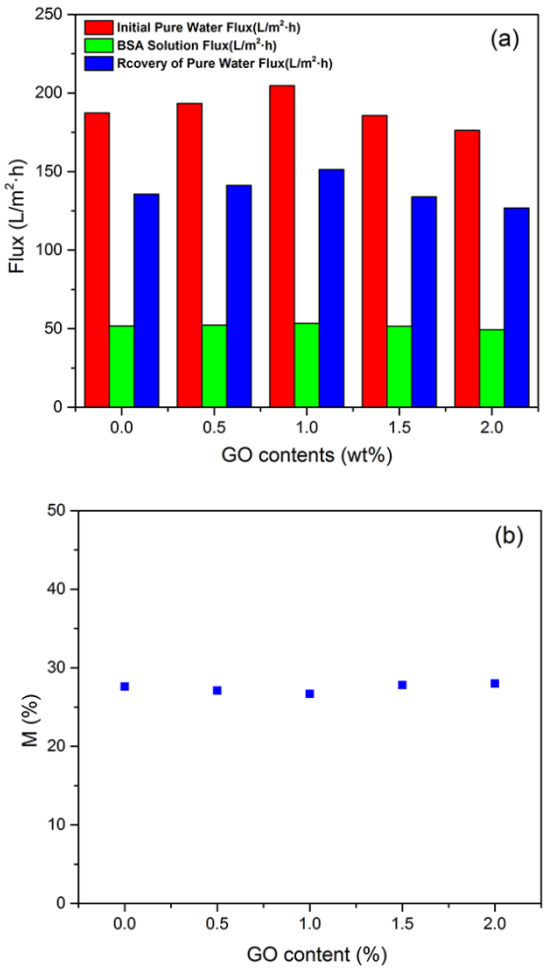

Fig. 9. (a) Permeation flux and (b) attenuation coefficient of the NCC/PVDF membrane and NCC/PVDF membranes containing 0.5, 1.0, 1.5, and 2.0 wt% GO.

shown in Fig. 2), but this interaction had certain effect on hydrophilicity of the GO/NCC/PVDF blend membrane [73]. Therefore, the synergetic effects of NCC and GO had no obvious improvement on the antipollution performance of PVDF UF membranes.

In addition, the comprehensive performance of GO/NCC/PVDF membranes in this work was compared against pure PVDF and GO/PVDF membranes from a recent literature, and the data are presented in Table 2. It indicated that the GO/NCC/PVDF membrane presented significantly upgraded the water permeability thermal stability and mechanical properties compared with the pure PVDF or GO/PVDF hybrid membranes, illustrating that such high-performance multifunctional membranes might broaden the horizon of membrane-based water and wastewater treatment technology.

4. Conclusion

Addition of GO obviously improved the mechanical properties and thermal stability of the NCC/PVDF membrane. The FTIR results showed that hydrogen bonds exist between GO and NCC, and the TEM revealed that GO and NCC is successfully dispersed in the blend membrane.

Table 2
Comparison of the comprehensive performance for PVDF and its GO modification hybrid membranes reported in the literatures and the GO/NCC-PVDF membrane in this work (the content of GO was based on the weight of PVDF)

Membrane	PVDF dosage (wt%)	GO dosage (wt%)	Tensile strength (MPa)	Contact angle (°)	Pure water flux (L/(m^2·h))	BSA rejection (%)	Attenuation coefficient (%)	Reference
PVDF	15	–	–	~87	~160	~70	~40	[47]
PVDF	15	–	4.62	–	121.2	~95	–	[24]
PVDF-GO	15	0.5	~4	~67	~50	~97	–	[20]
PVDF-GO	15	0.5	–	~68	104.3	85	~10	[47]
PVDF-GO	15	1.0	~2.5	~51	401.4	~55	~25	[57]
PVDF-GO/NCC	14	1.0	9.56	59.6	204.75	90.02	26.7	This work

The highest tensile strength and elongation-at-break of the GO/NCC/PVDF membrane were 9.56 MPa and 29.49%, which were 58.01% and 21.96% higher than those of the NCC/PVDF membrane, respectively. Furthermore, TGA indicated that the GO/NCC/PVDF membranes showed higher thermal stability than that of the NCC/PVDF membrane. Compared with the NCC/PVDF membrane, the T_{onest} and T_{max} of the GO/NCC/PVDF membrane were improved at 61°C and 26°C when the content of GO was 0.5 wt%. The pure water fluxes of the NCC/PVDF and GO/NCC/PVDF membranes were 187.32 and 204.75 L/(m2·h), respectively. The BSA rejections of the NCC/PVDF and GO/NCC/PVDF membranes were 91.04% and 90.02%, respectively. Thus, it could be concluded that the addition of GO did not have a remarkable effect on the pure water flux and BSA rejection. Furthermore, the attenuation coefficients of the blend membrane with and without addition of GO were both approximately 27%. Considering the above results, the high-performance multifunctional hybrid UF GO/NCC/PVDF membranes had potential applications, such as fouling mitigation in practical water treatment and suffer from greater pressure difference, thus improved the service life of the blend membrane in different environment.

Acknowledgment

The authors thank the Key Projects in the National Science and Technology Pillar Program during the 13th Five-year Plan Period (2017YFD0600804) for financial support of this work.

References

[1] B.S. Lalia, V. Kochkodan, R. Hashaikeh, N. Hilal, A review on membrane fabrication: structure, properties and performance relationship, Desalination, 326 (2013) 77–95.
[2] V.K. Thakur, S.I. Voicu, Recent advances in cellulose and chitosan based membranes for water purification: a concise review, Carbohydr. Polym., 146 (2016) 148–165.
[3] P. Qu, H. Tang, Y. Gao, S. Wang, Polyethersulfone composite membrane blended with cellulose fibrils, BioResources, 5 (2010) 2323–2336.
[4] H.D. Raval, J.M. Gohil, Carbon nanotube membrane for water desalination, Int. J. Nucl. Desal., 3 (2009) 360–368.
[5] H.D. Raval, B.B. Mehta, R.N. Joshi, A novel low-fouling zeolite-polysulfone nanocomposite membrane for advanced water treatment, Desal. Wat. Treat., 88 (2017) 8–15.
[6] Q. Yang, N. Adrus, F. Tomicki, M. Ulbricht, Blends of functional polymeric hydrogels and porous membranes, J. Mater. Chem., 21 (2011) 2783–2811.
[7] J. Zhang, Z. Xu, W. Mai, X. Qian, Improved hydrophilicity, permeability, antifouling and mechanical performance of PVDF blend ultrafiltration membranes tailored by oxidized low-dimensional carbon nanomaterials, J. Mater. Chem. A, 1 (2013) 3101–3111.
[8] S.S. Chin, K. Chiang, A.G. Fane, The stability of polymeric membranes in a TiO_2 photocatalysis process, J. Membr. Sci., 275 (2006) 202–211.
[9] X. Cao, J. Ma, X. Shi, Z. Ren, Effect of TiO_2 nanoparticle size on the performance of PVDF membrane, Appl. Surf. Sci., 253 (2006) 2003–2010.
[10] Y. Ji-xiang, S. Wen-xin, Y. Shui-li, L. Yan, Influence of DOC on fouling of a PVDF ultrafiltration membrane modified by nano-sized alumina, Desalination, 239 (2009) 29–37.
[11] L. Yan, S. Hong, M.L. Li, Y.S. Li, Application of the Al_2O_3–PVDF nanocomposite tubular ultrafiltration (UF) membrane for oily wastewater treatment and its antifouling research, Sep. Purif. Technol., 66 (2009) 347–352.
[12] Y. Zhao, Z. Xu, M. Shan, X. Qian, Effect of graphite oxide and multi-walled carbon nanotubes on the microstructure and performance of PVDF membranes, Sep. Purif. Technol., 103 (2013) 78–83.
[13] Y. Shen, A.C. Lua, Preparation and characterization of mixed matrix membranes based on PVDF and three inorganic fillers (fumed nonporous silica, zeolite 4A and mesoporous MCM-41) for gas separation, Chem. Eng. J., 192 (2012) 201–210.
[14] S. Rajabzadeh, T. Maruyama, Y. Ohmukai, H. Matsuyama, Preparation of PVDF/PMMA blend hollow fiber membrane via thermally induced phase separation (TIPS) method, Sep. Purif. Technol., 66 (2009) 76–83.
[15] J. Jiang, L. Zhu, L. Zhu, Y. Xu, Surface characteristics of a self-polymerized dopamine coating deposited on hydrophobic polymer films, Langmuir, 27 (2011) 14180–14187.
[16] F. Liu, N.A. Hashim, Y. Liu, M.M. Abed, K. Li, Progress in the production and modification of PVDF membranes, J. Membr. Sci., 275 (2011) 1–27.
[17] M. Hadidi, A.L. Zydney, Fouling behavior of zwitterionic membranes: impact of electrostatic and hydrophobic interactions, J. Membr. Sci., 452 (2014) 97–103.
[18] D. Liu, D. Li, D. Du, X. Zhao, A. Qin, X. Li, C. He, Antifouling PVDF membrane with hydrophilic surface of terry pile-like structure, J. Membr. Sci., 493 (2015) 243–251.
[19] J. Zhang, Z. Xu, M. Shan, B. Zhou, Y. Li, B. Li, X. Qian, Synergetic effects of oxidized carbon nanotubes and graphene oxide on fouling control and anti-fouling mechanism of polyvinylidene fluoride ultrafiltration membranes, J. Membr. Sci., 448 (2013) 81–92.
[20] N. Meng, R.C.E. Priestley, Y. Zhang, H. Wang, X. Zhang, The effect of reduction degree of GO nanosheets on microstructure and performance of PVDF/GO hybrid membranes, J. Membr. Sci., 501 (2016) 169–178.
[21] H.D. Raval, J.M. Gohil, Nanotechnology in water treatment: an emerging trend, Int. J. Nucl. Desal., 4 (2010) 184–188.
[22] F. Hussain, M. Hojjati, M. Okamoto, R.E. Gorga, Polymer-matrix nanoblends, processing, manufacturing, and application: an overview, J. Compos. Mater., 40 (2006) 1511–1575.

[23] M. Henriksson, L.A. Berglund, Structure and properties of cellulose nanoblend films containing melamine formaldehyde, J. Appl. Polym. Sci., 106 (2007) 2817–2824.
[24] H. Bai, X. Wang, Y. Zhou, L. Zhang, Preparation and characterization of poly (vinylidene fluoride) composite membranes blended with nano-crystalline cellulose, Prog. Nat. Sci., 22 (2012) 250–257.
[25] S. Li, Y. Gao, H. Bai, L. Zhang, P. Qu, L. Bai, Preparation and characteristics of polysulfone dialysis composite membranes modified with nanocrystalline cellulose, BioResources, 6 (2011) 1670–1680.
[26] J.R.G. Navarro, U. Edlund, Surface-initiated controlled radical polymerization approach to enhance nanocomposite integration of cellulose nanofibrils, Biomacromolecules, 18 (2017) 1947–1955.
[27] H. Dong, E. Napadensky, J.A. Orlicki, J.F. Snyder, T.L. Chantawansri, A. Kapllarni, Cellulose nanofibrils and diblock copolymer complex: micelle formation and enhanced dispersibility, ACS Sustainable Chem. Eng., 5 (2016) 1264–1271.
[28] Y. Feng, X. Zhang, Y. Shen, K. Yoshino, W. Feng, A mechanically strong, flexible and conductive film based on bacterial cellulose/graphene nanocomposite, Carbohydr. Polym., 87 (2012) 644–649.
[29] D. Han, L. Yan, W. Chen, W. Li, P.R. Bangal, Cellulose/graphite oxide composite films with improved mechanical properties over a wide range of temperature, Carbohydr. Polym., 83 (2011) 966–972.
[30] Y. Manawi, V. Kochkodan, M.A. Hussein, M.A. Khaleel, M. Khraisheh, N. Hilal, Can carbon-based nanomaterials revolutionize membrane fabrication for water treatment and desalination?, Desalination, 391 (2016) 69–88.
[31] X. Wang, W. Xing, P. Zhang, L. Song, H. Yang, Y. Hu, Covalent functionalization of graphene with organosilane and its use as a reinforcement in epoxy blends, Compos. Sci. Technol., 72 (2012) 737–743.
[32] M.Y. Shen, C.F. Kuan, H.C. Kuan, C.H. Chen, J.H. Wang, M.C. Yip, C.L. Chiang, Preparation, characterization, thermal, and flame-retardant properties of green silicon-containing epoxy/functionalized graphene nanosheets blends, J. Nanomater., 2013 (2013) 22.
[33] M. Hu, B. Mi, Enabling graphene oxide nanosheets as water separation membranes, Environ. Sci. Technol., 47 (2013) 3715–3723.
[34] S. Stankovich, D.A. Dikin, R.D. Piner, K.A. Kohlhaas, A. Kleinhammes, Y. Jia, R.S. Ruoff, Synthesis of graphene-based nanosheets via chemical reduction of exfoliated graphite oxide, Carbon, 45 (2007) 1558–1565.
[35] P. Sun, M. Zhu, K. Wang, M. Zhong, J. Wei, D. Wu, H. Zhu, Selective ion penetration of graphene oxide membranes, ACS Nano, 7 (2012) 428–437.
[36] Y. Zhang, L. Liu, F. Yang, A novel conductive membrane with RGO/PVDF coated on carbon fiber cloth for fouling reduction with electric field in separating polyacrylamide, J. Appl. Polym. Sci., 133 (2016) 43597.
[37] X. Lin, X. Liu, J. Jia, X. Shen, J.K. Kim, Electrical and mechanical properties of carbon nanofiber/graphene oxide hybrid papers, Compos. Sci. Technol., 100 (2014) 166–173.
[38] R. Kabiri, H. Namazi, Surface grafting of reduced graphene oxide using nanocrystalline cellulose via click reaction, J. Nanopart. Res., 16 (2014) 2474.
[39] L. Zhang, G. Chen, H. Tang, Q. Chong, S. Wang, Preparation and characterization of blend membranes of polysulfone and microcrystalline cellulose, J. Appl. Polym. Sci., 112 (2009) 550–556.
[40] Z. Ma, D. Liu, Y. Zhu, Z. Li, Z. Li, H. Tian, H. Liu, Graphene oxide/chitin nanofibril composite foams as column adsorbents for aqueous pollutants, Carbohydr. polym., 144 (2016) 230–237.
[41] H. Kargarzadeh, M. Mariano, D. Gopakumar, I. Ahmad, S. Thomas, A. Dufresne, N. Lin, Advances in cellulose nanomaterials, Cellulose, 25 (2018) 2151–2189.
[42] O. Nechyporchuk, M.N. Belgacem, J. Bras, Production of cellulose nanofibrils: a review of recent advances, Ind. Crops Prod., 93 (2016) 2–25.
[43] M. Acik, C. Mattevi, C. Gong, G. Lee, K. Cho, M. Chhowalla, Y.J. Chabal, The role of intercalated water in multilayered graphene oxide, ACS Nano, 4 (2010) 5861–5868.
[44] M. Safarpour, V. Vatanpour, A. Khataee, Preparation and characterization of graphene oxide/TiO_2 blended PES nanofiltration membrane with improved antifouling and separation performance, Desalination, 393 (2016) 65–78.
[45] H. Kim, Y. Miura, C.W. Macosko, Graphene/polyurethane nanocomposites for improved gas barrier and electrical conductivity, Chem. Mater., 22 (2010) 3441–3450.
[46] G. Wang, B. Wang, J. Park, J. Yang, X. Shen, J. Yao, Synthesis of enhanced hydrophilic and hydrophobic graphene oxide nanosheets by a solvothermal method, Carbon, 47 (2009) 68–72.
[47] C. Xu, G. Wang, C. Xing, L.M. Matuana, H. Zhou, Effect of graphene oxide treatment on the properties of cellulose nanofibril films made of banana petiole fibers, BioResources, 10 (2015) 2809–2822.
[48] Z. Wang, H. Yu, J. Xia, F. Zhang, F. Li, Y. Xia, Y. Li, Novel GO-blended PVDF ultrafiltration membranes, Desalination, 299 (2012) 50–54.
[49] M. Gopiraman, K. Fujimori, K. Zeeshan, B.S. Kim, I.S. Kim, Structural and mechanical properties of cellulose acetate/graphene hybrid nanofibers: spectroscopic investigations, eXPRESS Polym. Lett., 7 (2013) 554–563.
[50] W. Ouyang, J. Sun, J. Memon, C. Wang, J. Geng, Y. Huang, Scalable preparation of three-dimensional porous structures of reduced graphene oxide/cellulose composites and their application in supercapacitors, Carbon, 62 (2013) 501–509.
[51] X. Chang, Z. Wang, S. Quan, Y. Xu, Z. Jiang, L. Shao, Exploring the synergetic effects of graphene oxide (GO) and polyvinylpyrrolidone (PVP) on poly (vinylylidenefluoride) (PVDF) ultrafiltration membrane performance, Appl. Surf. Sci., 316 (2014) 537–548.
[52] A. Bottino, G. Camera-Roda, G. Capannelli, S. Munari, The formation of microporous polyvinylidene difluoride membranes by phase separation, J. Membr. Sci., 57 (1991) 1–20.
[53] Z. Xu, T. Wu, J. Shi, K. Teng, W. Wang, M. Ma, J. Fan, Photocatalytic antifouling PVDF ultrafiltration membranes based on synergy of graphene oxide and TiO_2 for water treatment, J. Membr. Sci., 520 (2016) 281–293.
[54] T. Wu, B. Zhou, T. Zhu, J. Shi, Z. Xu, C. Hu, J. Wang, Facile and low-cost approach towards a PVDF ultrafiltration membrane with enhanced hydrophilicity and antifouling performance via graphene oxide/water-bath coagulation, RSC Adv., 5 (2015) 7880–7889.
[55] P. Rittigstein, R.D. Priestley, L.J. Broadbelt, J.M. Torkelson, Model polymer nanoblends provide an understanding of confinement effects in real nanoblends, Nat. Mater., 6 (2007) 278–282.
[56] H. Zhang, Z.G. Wang, Z.N. Zhang, J. Wu, J. Zhang, J.S. He, Regenerated-cellulose/multiwalled-carbon-nanotube blend fibers with enhanced mechanical properties prepared with the ionic liquid 1-allyl-3-methylimidazolium chloride, Adv. Mater., 19 (2007) 698–704.
[57] B. Wang, W. Lou, X. Wang, J. Hao, Relationship between dispersion state and reinforcement effect of graphene oxide in microcrystalline cellulose–graphene oxide blend films, J. Mater. Chem., 22 (2012) 12859–12866.
[58] L. Liu, Z. Shen, S. Liang, M. Yi, X. Zhang, S. Ma, Graphene for reducing bubble defects and enhancing mechanical properties of graphene/cellulose acetate composite films, J. Mater. Sci., 49 (2014) 321–328.
[59] L. Yu, Y. Zhang, B. Zhang, J. Liu, H. Zhang, C. Song, Preparation and characterization of HPEI-GO/PES ultrafiltration membrane with antifouling and antibacterial properties, J. Membr. Sci., 447 (2013) 452–462.
[60] L. Liu, Y. Gao, Q. Liu, J. Kuang, D. Zhou, S. Ju, Z. Zhang, High mechanical performance of layered graphene oxide/poly (vinyl alcohol) nanoblendfilms, Small, 9 (2013) 2466–2472.
[61] H. Rabiee, M.H.D.A. Farahani, V. Vatanpour, Preparation and characterization of emulsion poly(vinyl chloride) (EPVC)/TiO_2 nanocomposite ultrafiltration membrane, J. Membr. Sci., 472 (2014) 185–193.

[62] H. Zhao, L. Wu, Z. Zhou, L. Zhang, H. Chen, Improving the antifouling property of polysulfone ultrafiltration membrane by incorporation of isocyanate-treated graphene oxide, Phys. Chem. Chem. Phys., 15 (2013) 9084–9092.
[63] B.M. Ganesh, A.M. Isloor, A.F. Ismail, Enhanced hydrophilicity and salt rejection study of graphene oxide-polysulfone mixed matrix membrane, Desalination, 313 (2013) 199–207.
[64] M. Kumar, D. McGlade, M. Ulbricht, J. Lawler, Quaternized polysulfone and graphene oxide nanosheet derived low fouling novel positively charged hybrid ultrafiltration membranes for protein separation, RSC Adv., 5 (2015) 51208–51219.
[65] C. Ao, W. Yuan, J. Zhao, X. He, X. Zhang, Q. Li, C. Lu, Superhydrophilic graphene oxide@electrospun cellulose nanofiber hybrid membrane for high-efficiency oil/water separation, Carbohydr. Polym., 175 (2017) 216–222.
[66] Z. Xu, J. Zhang, M. Shan, Y. Li, B. Li, J. Niu, X. Qian, Organosilane-functionalized graphene oxide for enhanced antifouling and mechanical properties of polyvinylidene fluoride ultrafiltration membranes, J. Membr. Sci., 458 (2014) 1–13.
[67] K. Gao, Z. Shao, X. Wu, X. Wang, J. Li, Y. Zhang, F. Wang, Cellulose nanofibers/reduced graphene oxide flexible transparent conductive paper, Carbohydr. Polym., 97 (2013) 243–251.
[68] L.Y. Ng, A.W. Mohammad, C.P. Leo, N. Hilal, Polymeric membranes incorporated with metal/metal oxide nanoparticles: a comprehensive review, Desalination, 308 (2013) 15–33.
[69] X. Li, X. Fang, R. Pang, J. Li, X. Sun, J. Shen, L. Wang, Self-assembly of TiO_2 nanoparticles around the pores of PES ultrafiltration membrane for mitigating organic fouling, J. Membr. Sci., 467 (2014) 226–235.
[70] S. Ayyaru, Y.H. Ahn, Application of sulfonic acid group functionalized graphene oxide to improve hydrophilicity, permeability, and antifouling of PVDF nanocomposite ultrafiltration membranes, J. Membr. Sci., 525 (2017) 210–219.
[71] Y. Wang, T. Wang, Y. Su, F.B. Peng, H. Wu, Z.Y. Jiang, Remarkable reduction of irreversible fouling and improvement of the permeation properties of poly (ether sulfone) ultrafiltration membranes by blending with pluronic F127, Langmuir, 21 (2005) 11856–11862.
[72] V. Vatanpour, S.S. Madaeni, R. Moradian, S. Zinadini, B. Astinchap, Fabrication and characterization of novel antifouling nanofiltration membrane prepared from oxidized multiwalled carbon nanotube/polyethersulfone nanocomposite, J. Membr. Sci., 375 (2011) 284–294.
[73] J. Jiang, L. Zhu, L. Zhu, H. Zhang, B. Zhu, Y. Xu, Antifouling and antimicrobial polymer membranes based on bioinspired polydopamine and strong hydrogen-bonded poly(N-vinyl pyrrolidone), ACS Appl. Mater. Interfaces, 5 (2013) 12895–12904.